Hyperfine Interact (2018) 239: 50
https://doi.org/10.1007/s10751-018-1524-0

Precise determination of hyperfine interactions and second-order doppler shift in ^{149}Sm Mössbauer transition

Satoshi Tsutsui[1] · Ryo Masuda[2] · Yoshitaka Yoda[1] · Makoto Seto[2]

Published online: 13 November 2018
© Springer Nature Switzerland AG 2018

Abstract
We have succeeded in precisely determining the hyperfine interactions, particularly the isomer shifts, in the ^{149}Sm Mössbauer transition. The difference in the nuclear radii between the ground and excited states is critical for the determination of isomer shifts but is relatively small in ^{149}Sm. Therefore, the precise determination by ^{149}Sm Mössbauer spectroscopy is difficult. The recent development of synchrotron-radiation-based Mössbauer spectroscopy allows the isomer shifts to be determined more precisely than previously with the help of wellcollimated synchrotron radiation. In particular, the time-window effect assists the precise determination of hyperfine interactions in the ^{149}Sm Mössbauer transition because this effect enables us to measure spectra with higher energy resolution than natural linewidth determined by the lifetime of the excited states. Meanwhile, highenergy-resolution measurements to determine center shifts by SR-based Mössbauer spectroscopy enable us to observe the second-order Doppler shift, which has not been discussed, particularly for heavy Mössbauer nuclei. We have discussed the precise determination of isomer shifts and the observation of the second-order Doppler shift using ^{149}Sm synchrotron-radiation-based Mössbauer spectroscopy.

Keywords Synchrotron-radiation-based Mössbauer spectroscopy · Isomer shift · Second-order Doppler shift · ^{149}Sm Mössbauer effect · Time-window effect

1 Introduction

Hyperfine interactions are useful for understanding the physical and chemical properties of materials from a microscopic viewpoint. Since a hyperfine interaction is represented as

This article is part of the Topical Collection on *Proceedings of the 4th Mediterranean Conference on the Applications of the Mössbauer Effect (MECAME 2018), Zadar, Croatia, 27-31 May 2018*
Edited by Mira Ristic and Stjepko Krehula

✉ Satoshi Tsutsui
satoshi@spring8.or.jp

[1] Japan Synchrotron Radiation Research Institute (JASRI), SPring-8, Sayo, Hyogo 679-5198, Japan

[2] Institute for Integrated Radiation and Nuclear Science, Kyoto University, Kumatori, Osaka 590-0494, Japan

a product of electronic and nuclear terms, the precise determination of hyperfine interactions depends on the nuclear nature of probe nuclei as well as the energy or time resolution of the spectrometers used to investigate the physical and chemical properties of materials: the nuclear Zeeman splitting is the product of the nuclear magnetic moment and the hyperfine magnetic field reflecting the electronic magnetic moment; the nuclear quadrupole interaction is the product of the nuclear quadrupole moment and the electric field gradient due to chemical bonding, the occupation of the electronic orbit and so forth. Material scientists use the nuclear parameters of probe nuclei such as the nuclear magnetic moment, nuclear quadrupole moment and so on as constants for measuring spectra. To investigate the physical and chemical properties of materials, therefore, more precise measurements are required to determine the magnitude of hyperfine interactions, when the nuclear parameters are smaller.

Mössbauer spectroscopy is a useful technique for investigating hyperfine interactions that employs a nuclear transition through the Mössbauer effect. The precise determination of observed hyperfine interactions depends on the lifetime of the excited states in the probe nuclei as well as the nuclear parameters mentioned above. In Mössbauer spectroscopy, the lifetime of the excited states provide a limit to the energy resolution with which the hyperfine interaction can be observed because of the uncertainty principle. Therefore, the precise determination of hyperfine interactions is also affected by the nuclear nature of the lifetime. In ^{149}Sm Mössbauer spectroscopy, which is useful for investigating the physical and chemical properties of various Sm compounds in a wide temperature range, the determination of the isomer shift and quadrupole interaction may be affected by the nuclear nature of ^{149}Sm. The natural linewidth determined by the lifetime of the excited state, 11.0 nsec, is 1.60 mm / sec. This value is larger than the difference in the isomer shift values between the Sm^{2+} and Sm^{3+} states, ˜0.9 mm / sec between SmF_2 and SmF_3 for example [1, 2]. Meanwhile, the nuclear quadrupole moments in both the ground state ($I_{gd} = 7/2$) and excited state ($I_{ex} = 5/2$) are small.

In conventional Mössbauer spectroscopy using a radioactive source, the limit of the energy resolution with which the hyperfine interaction can be observed in principle depends on the lifetime of the excited state in the probe nuclei except in coincidence methods [3]. In addition, when Mössbauer spectra are measured with radioactive sources, the geometrical effects in spectrometers are not negligible because nuclear γ-rays are emitted isotropically. To determine the hyperfine interactions precisely observed by Mössbauer spectroscopy, consideration of the nuclear nature in the probe nuclei and the measuring geometry is required. Meanwhile, synchrotron radiation (SR) sources allow us to use well-collimated X-rays. In this sense, an SR source makes it possible not to change the nuclear nature but to improve the measuring geometry due to well-collimated X-rays produced by SR source.

Here, we briefly mention the importance of the ^{149}Sm Mössbauer transition for material science. Sm is an attractive element in solid state physics as well as an important element in permanent magnets as an industrial application. Sm has valence degrees of freedom, which are not allowed in all rare-earth elements, as well as magnetic degrees of freedom. ^{149}Sm Mössbauer spectroscopy using radioactive sources was established [4, 5] and first applied to the investigation of magnetism [6, 7] more than a half century ago. Recently, the valence degrees of freedom in Sm have become of interest to material scientists because of the discovery of unconventional heavy fermion behavior as a quantum critical behavior from the viewpoint of solid state physics [8–10]. Our recent studies using X-ray absorption spectroscopy (XAS) suggest that the valence degrees of freedom are important for understanding the heavy fermion behavior in some Sm intermetallics, suggesting that the Sm valence is fluctuating [11–13]. However, since the time window in XAS measurements is PHz order

[14, 15], it is difficult to conclude that the valence fluctuates only from XAS measurements. Since the time window in Mössbauer spectroscopy is MHz or GHz order [16, 17],[1] depending on the magnitude of the hyperfine interactions, it is useful for discussing the fluctuation originating from electronic states such as the valence fluctuation behavior through the hyperfine interaction.

The development of nuclear resonant scattering techniuqes enables us to perform Mössbauer spectroscopy in the energy domain using an SR source [18]. Since most of the incident X-rays are scattered by electrons, pulse X-rays with a certain time interval are required to distinguish the weak signals of nuclear resonant scattering, known as Mössbauer resonance using the SR source, from strong signals of electronic scattering. The X-rays provided by SR facilities are pulsed X-rays. To effectively observe signals from nuclear resonant scattering with X-rays provided by SR facilities, the choice of the X-ray pulse interval is an important factor, which depends on the lifetime of the probe nuclei. It is necessary to choose an operation appropriate to the lifetime of the excited state in the probe nuclei, even when SR-based Mössbauer spectroscopy is performed. This technique also enables us to measure Mössbauer spectra with higher energy resolution than the resolution limit of the natural linewidth in the energy defined by the lifetime of the excited state in the probe nuclei [19]. Concerning the ^{149}Sm Mössbauer transition, the methodology of SR-based Mössbauer spectroscopy has been established [20]. In this study, $^{149}Sm_2O_3$ at room temperature was chosen as an analyzer. To achieve good detection efficiency, the $^{149}Sm_2O_3$ analyzer and an avalanche photodiode (APD) were installed in the same vacuum chamber In addition, the spectral change due to the time-window effect in signal detection was investigated. In the present work, we have succeeded in observing the second-order Doppler shift in a relatively heavy nucleus of ^{149}Sm, which has not been previously discussed, as well as the precise determination of isomer shifts in $SmBe_{13}$, $SmTi_2Al_{20}$ and SmB_6 using ^{149}Sm SR-based Mössbauer spectroscopy.

2 Spectral simulation and estimation of signal intensity

2.1 Spectral shape and linewidth

A spectral simulation was carried out assuming the same parameters in Sm_2O_3 except for the distributed nuclear levels: the thickness of the sample is 200 μm; the isotropic ratio of ^{149}Sm is the natural abundance of 13.9%; the recoil-free fraction of the sample is identical to that of Sm_2O_3 at 300 K of 0.42 [21]. Since the spectral shape in SR Mössbauer spectroscopy is affected by the operation mode of the SR facilities, we consider the 203 bunch operation, 4-bunch x 84train operation and 11-bunch x 29-train operation of SPring-8 (http://www.spring8.or.jp/en/users/operationstatus/schedule/bunchmodes), all of which are fully available for nuclear resonant scattering as shown in Table 1. The time structure of the X-ray pulses in each operation is shown in Fig. 1. The spectral shape is affected by the time window used for measurements, i.e., the starting time and stopping time, as well as the

[1] A typical treatment of the fluctuating hyperfine interaction has been previously reported [16, 17]. Since the hyperfine interaction observed is usually as much as neV or less than μeV, the time window in Mössbauer spectroscopy is of MHz or GHz order. This coincidentally and approximately agrees with the lifetime of the excited states in Mössbauer isotopes. Although the equation given in a previous treatment [16, 17] is independent of the lifetime of the excited states, it is sometimes said that the time window of Mössbauer spectroscopy is equal to the lifetime in a rough estimation.

Table 1 Parameters in SPring-8 user operations for SR-based Mössbauer spectroscopy (http://www.spring8.or.jp/en/users/operationstatus/schedule/bunchmodes)

Operation mode	Number of bunches in a train	Interval of single bunches or trains (nsec)	Ring current (mA)
203 bunches	1	23.6	100
4-bunch × 84 train	4	51.1	100
11-bunch × 29 train	11	145.6	100

Note that interval between the bunches in each train is 1.97 nsec

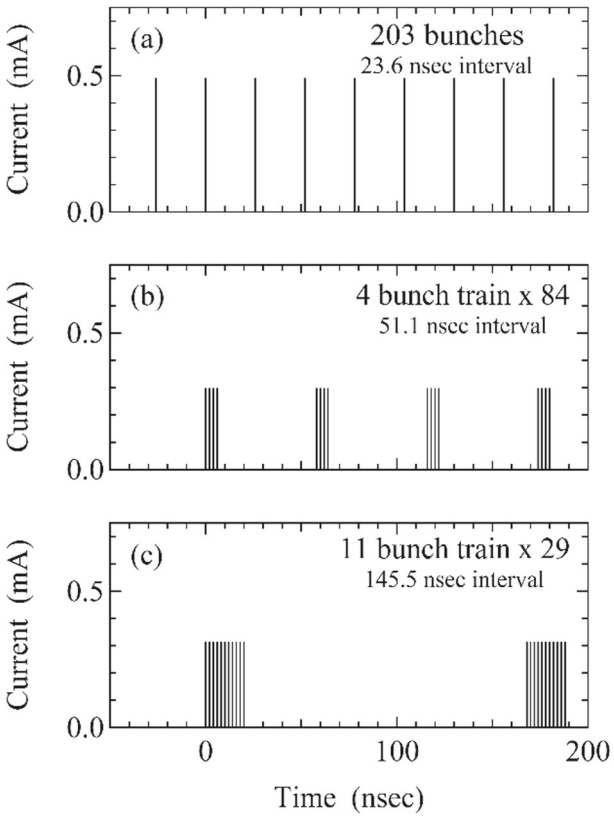

Fig. 1 Time structure of X-ray pulses in each operation mode of SPring-8 (http://www.spring8.or.jp/en/users/operationstatus/schedule/bunchmodes). The current in mA corresponds to the intensity of the X-ray pulse as a function of time in nsec.

operation mode of the SR facilities. Here, we define the starting time as the time when the signals of nuclear resonant scattering start to be measured after last X-ray pulse comes and the stopping time as the time when the measurement of the signals stops. The time window is defined as the time during which signals of nuclear resonant scattering are measured. In the present work, although the stopping time was fixed as the time immediately before the next X-ray pulse comes, the starting time was varied to change the energy resolution of

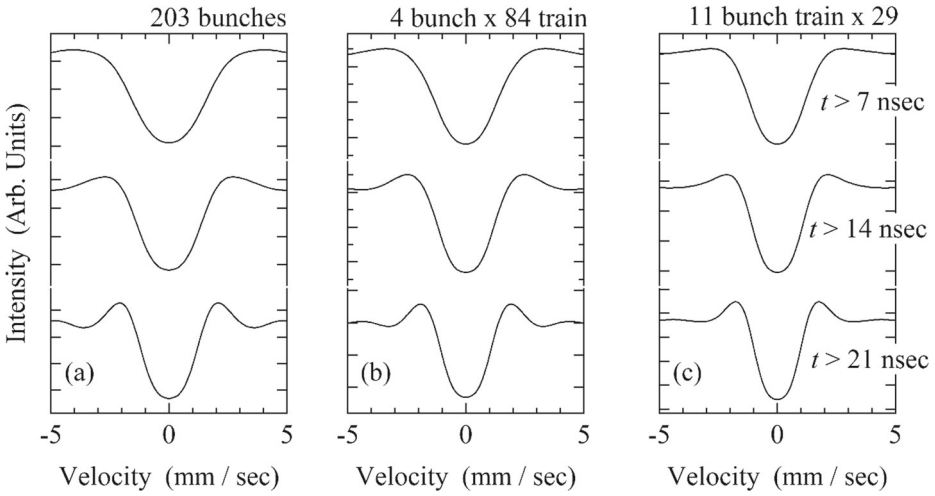

Fig. 2 Operation mode and time-window dependence of simulated spectra in ^{149}Sm SR-based Mössbauer spectroscopy

the spectral measurements and/or the detection efficiency of the signals of nuclear resonant scattering.

The simulated timewindow dependences of the spectral shape under the 203-bunch operation the 4-bunch × 84 train operation and 11-bunch × 29-train operation of SPring-8 are shown in Fig. 2a, b, c, respectively. As reported in Ref. [20], the spectral linewidth in the 11-bunch × 29-train operation is narrower than that in the 203-bunch operation for the same starting time, with that in the 4-bunch × 84 train operation between those of the 203-bunch and 11-bunch × 29-train operations (http://www.spring8.or.jp/en/users/operationstatus/schedule/bunchmodes). Meanwhile, the starting-time dependence of the spectral linewidth is qualitatively similar between the 203-bunch and 11-bunch × 29-train operations in SPring-8. The resonance linewidth becomes increasingly narrower as the starting time becomes later. The background oscillation and tail structure become increasingly complicated in all cases. The background oscillation is more apparent in the 203-bunch operation, whereas the tail structure is steeper in the 11-bunch × 29-train operation (http://www.spring8.or.jp/en/users/operationstatus/schedule/bunchmodes). However, the peak position, which is important for discussing the hyperfine interaction, is insensitive to the time-window effect in spite of the changing peak shape. These simulation results demonstrate that the time-window effect of SR Mössbauer spectra is very useful for precisely determining the hyperfine interaction, regardless of the operation mode in the SR facility.

We also consider the startingtime dependence of the spectral linewidth in our simulation results for the sample shown in Fig. 2. When simulated spectra are fitted with a single Lorentzian function to determine the linewidth of the resonance absorption, the startingtime dependence of the simulated spectra in each operation mode shown in Fig. 3 is obtained. The startingtime dependence of the spectral linewidth is stronger in the 203-bunch operation than in the other operations. The spectral linewidth exponentially decreases with increasing starting time. Since the interval between each X-ray pulse is 23.6 nsec in the 203-bunch operation, measurement with a starting time later than 24 nsec is impossible. When we set the starting time to 21 nsec, the signal rate is predicted to be very limited in the 203-bunch

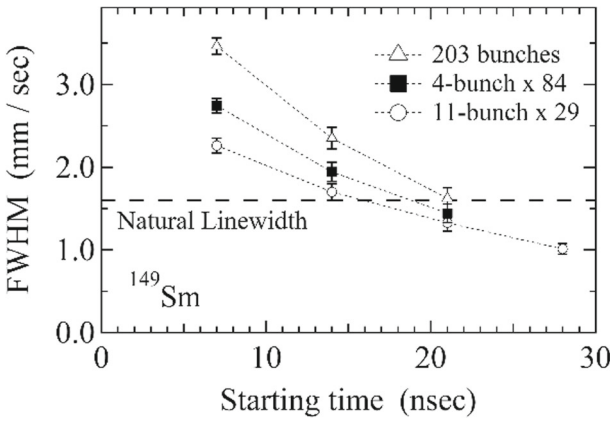

Fig. 3 Plots of linewidth against starting time for counting signals of ^{149}Sm SR-based Mössbauer spectra in various SPring-8 operation modes. Linewidths were obtained by the spectral analyses of simulated spectra shown in Fig. 2 using a single Lorentzian function. The dashed line depicts the natural linewidth of the ^{149}Sm Mössbauer resonance

operation of SPring-8, resulting in very limited signal rates. As shown in Fig. 3, the spectral linewidth obtained in the 203bunch operation is close to that in the 4-bunch × 84train and 11-bunch × 29-train operations. The linewidth obtained from the data for the 4-bunch × 84-train operation is between those obtained for the 203bunch operation and 11-bunch × 29-train operation. The linewidth also depends on the sample thickness as has been observed in conventional Mössbauer spectroscopy using both radioactive and SR sources.

2.2 Detection efficiency

The detection efficiency of signals is also an experimentally important factor in the measurement of spectra. Since the intensity of nuclear resonant signals exponentially decays as a function of time after the excitation of nuclei by X-rays, the operation mode dependence of the detection efficiency should be considered when carrying out SR-based Mössbauer spectroscopy. We estimated the detection efficiency of signal rate in SR-based Mössbauer spectroscopy when the time window used for signal detection is open as wide as possible in each operation.

The detection efficiency of nuclear resonance signals in the three operation modes of the 203-bunch operation, 4-bunch × 84 train operation and 11-bunch × 29-train operation (http://www.spring8.or.jp/en/users/operationstatus/schedule/bunchmodes) is shown in Table 2 assuming the absence of multiple excitations in the nuclear resonance. The detection efficiency is nearly identical for the 203-bunch operation and 4-bunch × 84train operation and much higher than that for the 11-bunch × 29-train operation. When we consider both the linewidth and detection efficiency, the 4-bunch × 84-train operation is the best mode for carrying out ^{149}Sm SR-based Mössbauer spectroscopy. When the time window is reduced to reduce the linewidth for a high-energy resolution setup, the signal rate for the SR-based Mössbauer spectroscopy can be reduced by setting the starting time later. When the starting time is chosen to be after 20 nsec in 4-bunch × 84-train or 11-bunch × 29train operation, the simulation results suggest that higher energy resolution can be achieved in ^{149}Sm SR-based Mössbauer measurements.

Table 2 Operation mode dependence of detection efficiency in ^{149}Sm SR-based Mössbauer spectroscopy when the signals from nuclear resonant scattering are taken at 7 nsec after the last X-ray pulse comes into detector. Detection efficiencies were normalized by that for the 11-bunch x 29-train operation in SPring-8 (http://www.spring8.or.jp/en/users/operationstatus/schedule/bunchmodes)

Operation mode in SPring-8	Normalized detection efficiency
203-bunch operation	1.7
4-bunch x 84-train operation	1.6
11-bunch x 29-train operation	1

3 Experimental results

3.1 Experimental procedure

^{149}Sm SR-based Mössbauer spectroscopy was carried out at BL09XU in SPring-8. The details were reported in Ref. [20]. A high resolution monochromator (HRM) which consists of Si(4 2 2) and Si(16 8 8) crystals is located after the Si(1 1 1) doublecrystal monochromator in the beamline. The HRM improves the signal to noise ratio and reduces the energy band-width of X-ray to 1.5 meV at 22.507 keV. Measured samples were located in the upstream of the beamline at a distance of about 7 m from the $^{149}Sm_2O_3$ analyzer. In addition, the installation of a detector into the vacuum chamber that includes the $^{149}Sm_2O_3$ analyzer mounted on a velocity transducer improves the counting rate of nuclear resonant signals owing to the detection of internal conversion electrons as well as resonant X-rays [22].

As discussed in the previous section, the 4-bunch × 84-train operation is the best operation for ^{149}Sm SR-based Mössbauer spectroscopy from the viewpoints of scattering intensity and linewidth (http://www.spring8.or.jp/en/users/operationstatus/schedule/bunchmodes). In the present work, the 4-bunch × 84-train operation was chosen to perform ^{149}Sm SR-based Mössbauer spectroscopy on several compounds.

3.2 Experimental results for $SmBe_{13}$ and $SmTi_2Al_{20}$

$SmBe_{13}$ and $SmTi_2Al_{20}$ are magnetic compounds: $SmBe_{13}$ undergoes an antiferromagnetic ordering at 9 K [23]; $SmTi_2Al_{20}$ also undergoes an antiferromagnetic ordering at 6 K [9, 24]. Magnetic susceptibility measurement of $SmBe_{13}$ demonstrates that the Sm valence state is a purely trivalent state [25] and that of $SmTi_2Al_{20}$ suggests that the Sm valence state is an intermediate state between divalent and trivalent states [9]. The Sm valence state in $SmTi_2Al_{20}$ has been confirmed as an intermediate, which is also confirmed by XAS [13]. A common feature of these compounds is their cubic symmetry at the Sm site [25–28], which indicates the absence of nuclear quadrupole interactions in these compounds. In the present work, ^{149}Sm SR-based Mössbauer spectroscopy was performed on $SmBe_{13}$ and $SmTi_2Al_{20}$ at various temperatures with a high-resolution setup using the time-window effect.

Figure 4a and b respectively show ^{149}Sm SR-based Mössbauer spectra of $SmBe_{13}$ and $SmTi_2Al_{20}$ in their paramagnetic states. The SR-based Mössbauer measurements were carried out with a high energy-resolution setup, whose starting time was chosen as 20 nsec. The observed spectra reflect cubic symmetry at the Sm site: single line spectra were observed

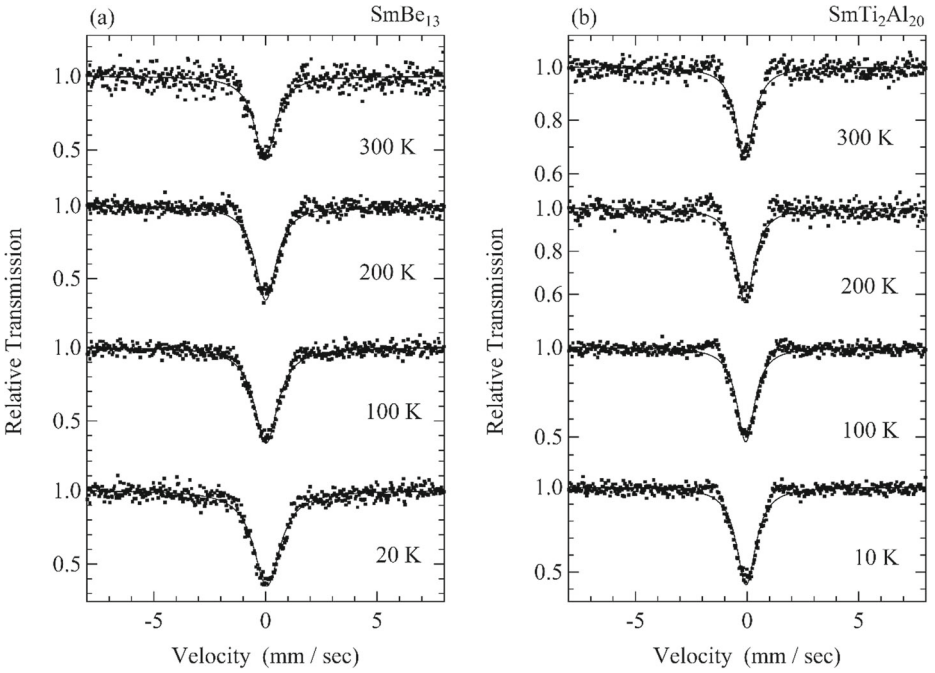

Fig. 4 ^{149}Sm SR-based Mössbauer spectra of **a** $SmBe_{13}$ and **b** $SmTi_2Al_{20}$ at various temperatures in their paramagnetic states

in their paramagnetic states. As expected from the results of magnetic susceptibility measurements, the spectra at 300 K demonstrate that the Sm valence state in $SmTi_2Al_{20}$ is an intermediate valence state or that it fluctuates between the Sm^{2+} and Sm^{3+} states, whereas that in $SmBe_{13}$ is a purely Sm^{3+} state. Spectral analyses with a single Lorentzian function provide the temperature dependence of the center shift in each compound. The center shift in both compounds exhibits a linear temperature dependence as shown in Fig. 5. These experimental findings suggest that the valence states in both compounds exhibit temperature dependence but disagree with the previous results based on magnetic susceptibility [9, 23, 25] and XAS [13], if the center shifts in these compounds are affected only by the Sm valence state.

In general, the center shift is connected with both the isomer shift due to the valence states and the second-order Doppler shift due to phonons. Since the second-order Doppler shift in heavy nuclei such as ^{149}Sm has been seldom discussed, change in the center shift value in heavy nuclei is usually recognized as that in the valence state. Considering the small difference in the isomer shift between Sm^{2+} and Sm^{3+} states in the ^{149}Sm Mössbauer effect as well as the experimental results based on magnetic susceptibility and XAS measurements, the contribution of the second-order Doppler shift to the center shift is worth considering when the temperature dependence of the center shifts in $SmBe_{13}$ and $SmTi_2Al_{20}$ is interpreted. In particular, the disagreement between the present work and previous magnetic susceptibility and XAS measurements infers that the effect of the second-order Doppler shift is not negligible. Since the Sm valence state in $SmBe_{13}$ is expected to be a purely trivalent state from the magnetic susceptibility measurement [23, 25], no temperature dependence of the Sm valence state is expected. The temperature dependence of the Sm valence state in

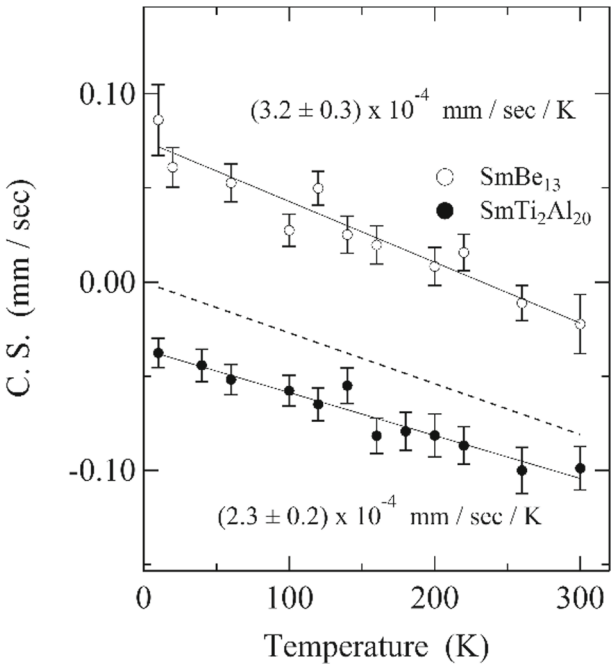

Fig. 5 Temperature dependence of center shift in ^{149}Sm SR-based Mössbauer spectra of $SmBe_{13}$ and $SmTi_2Al_{20}$. Solid lines are the fitting results for each compound. The dotted line shows slope of the limit at high temperature

$SmTi_2Al_{20}$ was also unexpected because the XAS spectra show no temperature dependence [13]. However, linear temperature dependence of the center shift was observed for both $SmBe_{13}$ and $SmTi_2Al_{20}$ as shown in Fig. 5. In this sense, the contribution of the change in the isomer shift to the center shift can be excluded when explaining the linear temperature dependence of the center shifts observed in both $SmBe_{13}$ and $SmTi_2Al_{20}$. In other words, the linear temperature dependence could be caused by the second-order Doppler shift.

3.3 Experimental results for SmB_6

SmB_6 is known as a valence-fluctuating system. Mössbauer spectroscopy on SmB_6 was first performed about a half century ago [1, 2]. These works suggest that the Sm valence state is between the Sm divalent and trivalent states but the isomer shift exhibits no temperature dependence. The previous reported spectra of SmB_6 at various temperatures suggest the absence of a nuclear quadrupole interaction reflecting the cubic symmetry at the Sm site [29]. Meanwhile, the Sm valence state estimated by XAS measurements and from its thermal expansion including neutron diffraction suggested that the Sm valence state in SmB_6 exhibits temperature dependence [30–32]. These results contradict the previous results obtained by Mössbauer spectroscopy. Since the natural linewidth of ^{149}Sm Mössbauer effect is too broad to discuss the precise Sm valence state in Sm compounds as mentioned above, such a natural linewidth and/or geometrical effect in measurements might have prevented the detection of the temperature dependence of the isomer shift in the previous studies.

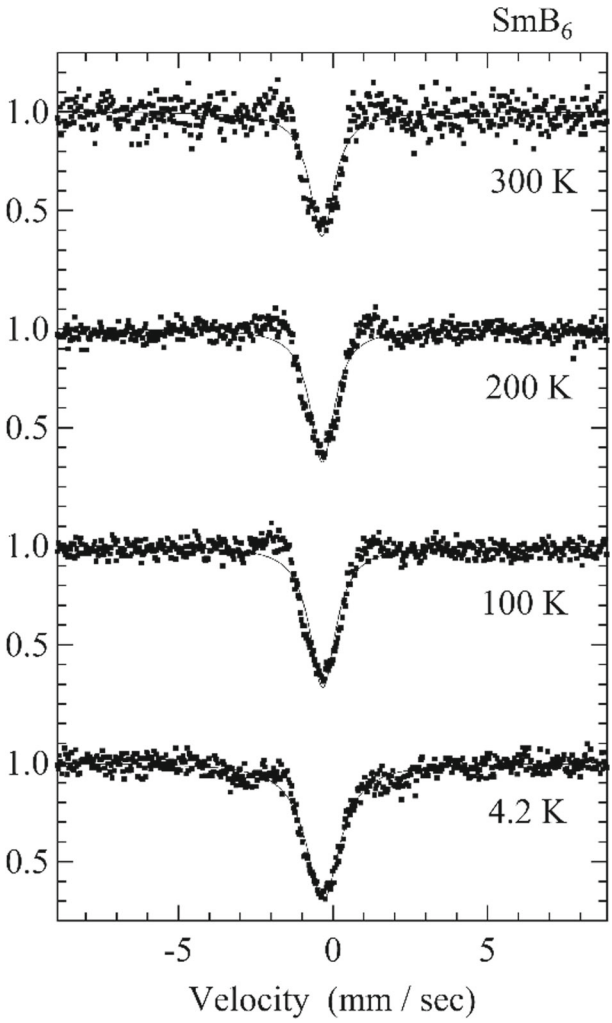

Fig. 6 ^{149}Sm SR-based Mössbauer spectra of polycrystalline SmB_6 at various temperatures. Solid curves are fitting results obtained using a Lorentzian function

^{149}Sm SR-based Mössbauer spectra of SmB_6 obtained using a polycrystalline sample are shown in Fig. 6. The SR-based Mössbauer measurements were carried out with a high energy-resolution setup, whose starting time was chosen as 20 nsec. All the spectra were successfully fitted with a single Lorentzian function except for the tail of the resonant absorption owing to the time-window effect. This spectral analysis provides the temperature dependence of the center shift as shown in Fig. 7. Unlike the previous results of ^{149}Sm Mössbauer spectroscopy [1, 2], the evident temperature dependence of the center shift can be seen in SmB_6. This may have been caused by the wellcollimated beam of SR X-rays as well as the high-resolution measurements based on the time-window effect in SR-based Mössbauer spectroscopy. The observed temperature dependence has steplike behavior

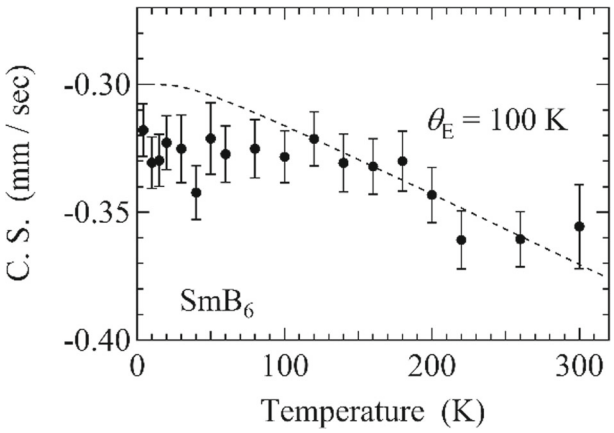

Fig. 7 Temperature dependence of center shift in ^{149}Sm SR-based Mössbauer spectra of SmB_6 obtained using a powder sample. The dotted curve represents a calculation based on the Einstein model

below about 180 K. However, the characteristic temperature based on the center shift is difficult to explain only from the temperature dependence of the Sm valence state estimated by XAS measurements [30]. The characteristic temperature estimated by XAS measurements is about 140 K, in agreement with the temperature at which anomaly in the thermal expansion was observed in neutron diffraction experiments. Therefore, as discussed in the results for $SmBe_{13}$ and $SmTi_2Al_{20}$, the contribution of second-order Doppler shift to the center shift appears to be essential to interpret the experimental results for SmB_6. When we considered the effect of the second-order Doppler shift on the center shift, the characteristic temperature of the Sm valence state estimated from the center shift agreed well with that estimated by XAS measurements as shown in Fig. 7.

We also measured a single-crystalline SmB_6 sample. The thickness of the measured sample was 200 μm. The incident X-rays were parallel to the [1 0 0] direction. In this measurement, we found a fine structure in the peaks as shown in Fig. 8. The fine structure was caused by the difference in the transition probability between a powder pattern and a single-crystalline one, but the origin of the fine structure owing to observation of nuclear quadrupole interaction, several Sm valence states and so forth has not yet been confirmed. Assuming that the fine structure is caused by the nuclear quadrupole interaction corresponding to the transition from the 7/2 state to the 5/2 state in the ^{149}Sm Mössbauer transition, we successfully fitted the results using a set of eight Lorentzian functions. Under this assumption, the temperature dependence of the center shift agrees with the results using a polycrystalline sample except for a shift due to the consideration of the nuclear quadrupole interaction. The origin of the nuclear quadrupole interaction is perhaps the electric field gradient produced by an electronic quadrupole moment or the orbital occupancy of Sm 4f electrons, but this has not yet been clarified. This nuclear quadrupole interaction does not exhibit any temperature dependence.

4 Discussion

When the second-order Doppler shift is calculated using the Debye and Einstein models based on the ^{149}Sm Mössbauer resonance, the temperature dependence is very close to that

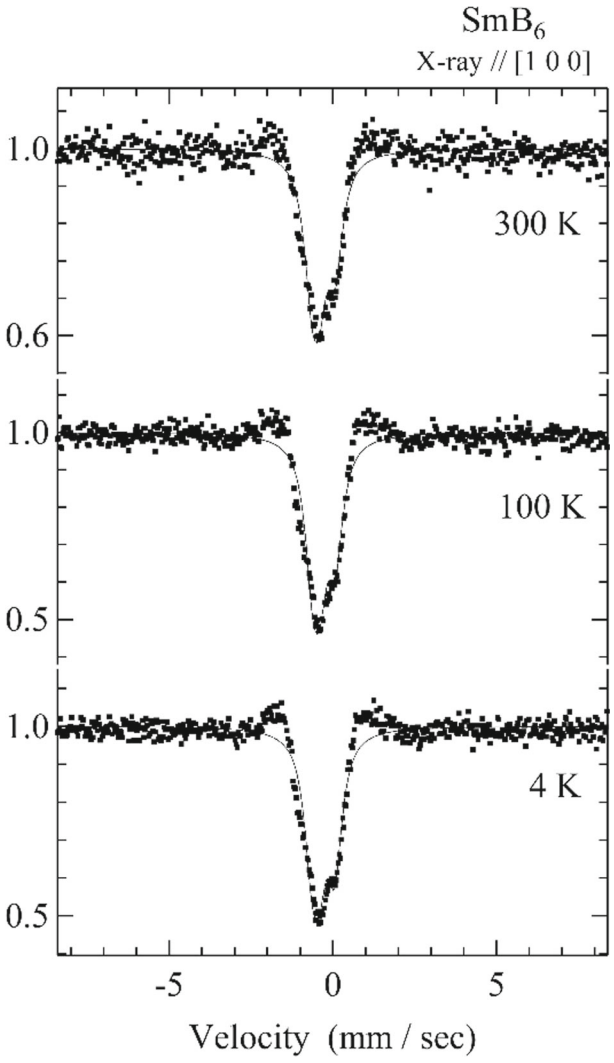

Fig. 8 ^{149}Sm SR-based Mössbauer spectra of single-crystalline SmB_6 at various temperatures. Solid curves are fitting results obtained using a set of eight Lorentzian functions

obtained with each model as shown in Fig. 9 except for the difference between the Debye and Einstein temperatures. The second-order Doppler shift exhibits a linear temperature dependence, which is a typical behavior as the high temperature limit for each Mössbauer nucleus, as shown in Fig. 9. Although we have no information on the phonon dispersion or the lattice dynamic parameters such as the Debye or Einstein temperature for $SmTi_2Al_{20}$, the phonon dispersion relation and the Einstein temperature at the Sm site are known for both $SmBe_{13}$ and SmB_6: the Einstein temperature at the Sm site in $SmBe_{13}$ has been estimated to be about 150 K by X-ray diffraction [27] and inelastic X-ray scattering [33]; the

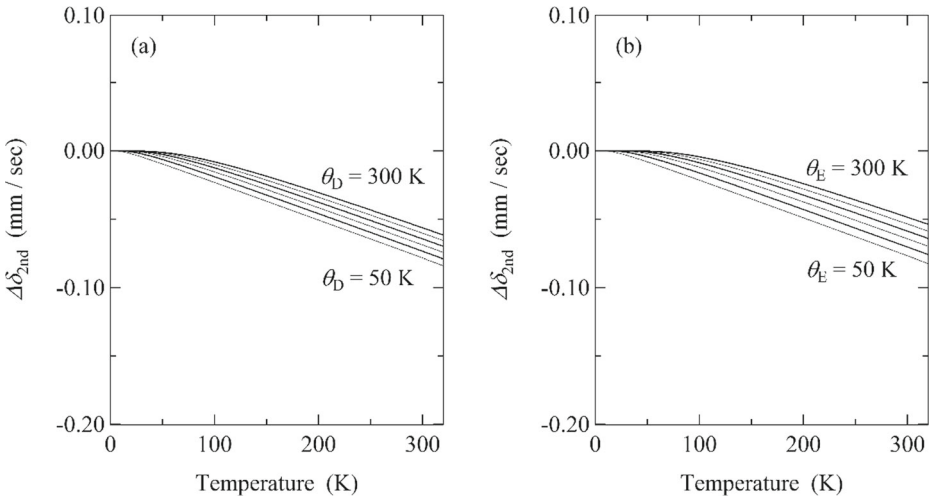

Fig. 9 Calculation of the second-order Doppler shift using **a** Debye and **b** Einstein models based on ^{149}Sm Mössbauer transition. The calculation was performed at interval of 50 K of the Debye or Einstein temperature. Bold curves correspond to Debye or Einstein temperatures of 100, 200 and 300 K

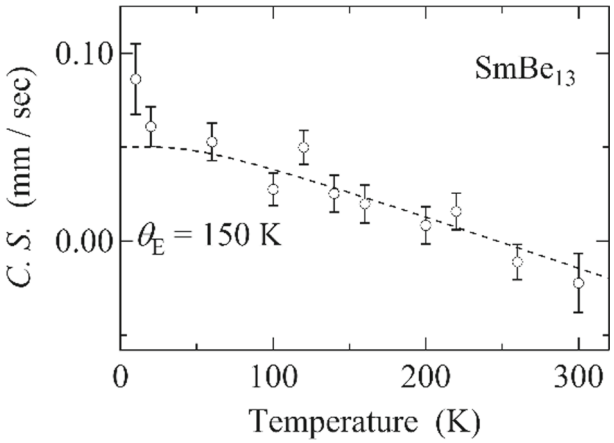

Fig. 10 Temperature dependence of center shift in $SmBe_{13}$. The dotted curve represents the result calculated with the Einstein model

Einstein temperature at the Sm site in SmB_6 is 100 K [34, 35]. This means that more detailed discussion is possible for $SmBe_{13}$ and SmB_6.

The temperature dependence of the center shift in $SmBe_{13}$ is simpler than that in SmB_6 because Sm valence state expected to be unchanged as a function of temperature Linear temperature dependence above 100 K demonstrates that the Sm valence state is unchanged as expected from macroscopic measurements [23, 25]. Since the linear dependence of the center shift was observed in the whole temperature region of the paramagnetic state, the observed deviation from the calculated curve based on the Einstein model shown in Fig. 10

implies that the hybridization between 4f and conduction electrons might be important when considering the ground state of $SmBe_{13}$. On the other hand, although the temperature dependence of the Sm valence state is more complicated in SmB_6 than in $SmBe_{13}$, the interpretation of the temperature dependence is much simpler for SmB_6 than for $SmBe_{13}$. When we attempted to fit the observed data with a calculated curve based on the Einstein model in high-temperature region, higher than 100 K, the deviation from the calculated curve was caused by the change in the Sm valence state as discussed for the previous XAS and neutron diffraction results shown in Fig. 7 [30, 31]. The constant behavior in the low temperature region, below about 20 K, is interpreted to be due to the unchanged isomer shift with the changing Sm valence state or to the small change within the experimental error, because abnormal thermal expansion associated with the change in the Sm valence state was reported [30, 32]. The effect of the change in the Sm valence on the isomer shift in the ^{149}Sm Mössbauer spectra is smaller at about 120 K, than at about 30 K.

From the viewpoint of precise determination of the hyperfine interaction, the center shift was observed on the basis of the coupling between the isomer shift and the second-order Doppler shift. The second-order Doppler shift is based on the phonon dispersion relation and/or phonon density of states associated with the probe atomic site. Even if the phonon dispersion relation and/or phonon density of states is unknown, a phonon calculation based on the crystal structure could be used as a reference to estimate the magnitude of the second-order Doppler shift. Since SR-based Mössbauer spectroscopy can in principle be applied to all the Mössbauer isotopes, precise determination is possible even for Mössbauer isotopes other than the ^{149}Sm isotope as discussed in the present work.

5 Summary

We have succeeded in the precise determination of the isomer shift using ^{149}Sm SR-based Mössbauer spectroscopy, which is an important parameter for discussing Sm valence state in the Sm intermetallics of $SmBe_{13}$, $SmTi_2Al_{20}$ and SmB_6. The good collimation of X-rays delivered by an SR source as well as the development of SR-based Mössbauer spectroscopy enabled us to observe the temperature dependence of the isomer shift, which was difficult to discuss previously. At the same time, the second-order Doppler shift was successfully observed in heavy ^{149}Sm nuclei, which is generally negligible in measurements of Mössbauer spectra using heavy nuclei. Meanwhile, since the isomer shift are always coupled with the second-order Doppler shift, careful data treatment is required to estimate the isomer shift even in heavy Mössbauer isotopes, particularly with high-resolution measurements using the time-window effect.

Although high-resolution measurements using the time-window effect in SR-based Mössbauer spectroscopy provide unexpected effects such as the second-order Doppler shift in the heavy Mössbauer isotope of ^{149}Sm, such high-resolution measurement is also helpful for determining the magnitudes of the hyperfine magnetic field and nuclear quadrupole interaction even in Mössbauer nuclei having small nuclear magnetic and/or quadrupole moments. For example, the small nuclear quadrupole moments in ^{151}Eu as well as ^{149}Sm may make it difficult to determine the nuclear quadrupole interactions in some Sm or Eu compounds using conventional Mössbauer spectroscopy with radioactive sources. Since SR-based Mössbauer spectroscopy is in principle applicable to all the Mössbauer isotopes, this technique could be helpful for Mössbauer isotopes such as ^{151}Eu.

Acknowledgements The authors appreciate Yoshio Kobayashi, Jin Nakamura, Shota Amagasa, Yasuhiro Yamada, Michael K. Kubo, Wataru Sato, Yasuhiro Kobayashi, and Hisao Kobayashi for their experimental assistance of ^{149}Sm SR Mössbauer spectroscopy. The authors also appreciate Akira Yamada, Ryuji Higashinaka, Tatsuma D. Matsuda, Yuji Aoki, Yusei Shimizu, Hiroyuki Hidaka, Tatsuya Yanagisawa, Hiroshi Amitsuka, and Fumitoshi Iga for the preparation of high quality samples. The present work was carried out under the approval of JASRI (2015A2036, 2015B1947, 2016A1281, 2016B1057, 2016B1967, 2017A1060, 2017B1275). This work was partially supported by Grants-in-Aid for Scientific Research B (15H03697) and Challenging Exploratory Research (15K14170).

References

1. Cohen, R.L., Eibschütz, M., West, K.W.: Phys. Rev. Lett. **24**, 383 (1970)
2. Eibschutz, M., Cohen, R., Buehler, E., Wernick, J.: Phys. Rev. B **6**, 18 (1972)
3. Hamill, D.W., Hoy, G.R.: Phys. Rev. Lett. **21**, 724 (1968)
4. Alfimenkov, V.P., Ostanevich, Y.M., Ruskov, T., Strelkov, A.V., Shapiro, F.L., Kuang, Y.: Sov. Phys. JETP **15**, 718 (1962)
5. Jha, S., Segnan, R., Lang, G.: Phys. Lett. **2**, 117 (1962)
6. Ofer, S., Segal, E., Nowik, I., Bauminger, E.R., Grodzins, L., Freeman, A.J., Schieber, M.: Phys. Rev. **137**, A627 (1965)
7. Ofer, S., Nowik, I.: Nucl. Phys. **A93**, 689 (1967)
8. Sanada, S., Aoki, Y., Aoki, H., Tsuchiya, A., Kikuchi, D., Sugawara, H., Sato, H.: J. Phys. Soc. Jpn. **74**, 246 (2005)
9. Higashinaka, R., Maruyama, T., Nakama, A., Miyazaki, R., Aoki, Y., Sato, H.: J. Phys. Soc. Jpn. **80**, 390703 (2011)
10. Sakai, A., Nakatsuji, S.: Phys. Rev. B **84**, 201106 (2011)
11. Mizumaki, M., Tsutsui, S., Tanida, H., Uruga, T., Kikuchi, D., Sugawara, H., Sato, H.: J. Phys. Soc. Jpn. **76**, 053706 (2007)
12. Tsutsui, S., Kawamura, N., Mizumaki, M., Ishimatsu, N., Maruyama, H., Sugawara, H., Sugawara, H., Sato, H.: J. Phys. Soc. Jpn. **82**, 023707 (2013)
13. Higashinaka, R., Yamada, A., Miyazaki, R., Aoki, Y., Mizumaki, M., Tsutsui, S., Nitta, K., Uruga, T., Sato, H.: JPS Conf. Proc. **3**, 011079 (2014)
14. Teo, B.K.: EXAFS: Basic Principles and Data Analysis. Springer, Berlin (1986)
15. Keski-Rahkonen, O., Krause, M.O.: At. Data Nucl. Data Tables **14**, 139 (1974)
16. Wickmann: In: Gruvermann (ed.) Mössbauer Methodology, vol. 2. Plenum Press, New York (1966)
17. Blume, M., Tjon, J.A.: Phys. Rev. **165**, 446 (1968)
18. Seto, M., Masuda, R., Higashitaniguchi, S., Kitao, S., Kobayashi, Y., Inaba, C., Mitsui, T., Yoda, Y.: Phys. Rev. Lett. **102**, 217602 (2009)
19. Seto, M., Masuda, R., Higashitaniguchi, S., Kitao, S., Kobayashi, Y., Inaba, C., Mitsui, T., Yoda, Y.: J. Phys. Conf. Ser. **217**, 012002 (2010)
20. Tsutsui, S., Masuda, R., Kobayashi, Y., Yoda, Y., Mizuuchi, K., Shimizu, Y., Hidaka, H., Yanagisawa, T., Amitsuka, H., Iga, F., Seto, M.: J. Phys. Soc. Jpn. **85**, 083704 (2016)
21. Rölsberger, R., Quast, K.W., Toellner, T.S., Lee, P.L., Sturhahn, W., Alp, E.E., Burkel, E.: Phys. Rev. Lett. **87**, 047601 (2001)
22. Masuda, R., Kobayashi, Y., Kitao, S., Kurokuzu, M., Saito, M., Yoda, Y., Mitsui, T., Iga, F., Seto, M.: Appl. Phys. Lett. **104**, 082411 (2014)
23. Hidaka, H., Yamazaki, S., Shimizu, Y., Miura, N., Tabata, C., Yanagisawa, T., Amitsuka, H.: J. Phys. Soc. Jpn. **86**, 074703 (2017)
24. Tsutsui, S., Kobayashi, Y., Nakamura, J., Kubo, M.K., Amagasa, S., Yamada, Y., Yoda, Y., Shimizu, Y., Hidaka, H., Yanagisawa, T., Amitsuka, H., Yamada, A., Higashinaka, R., Matsuda, T.D., Aoki, Y.: Hyperfine Int. **238**, 100 (2017)
25. Bucher, E., Maita, J.P., Hull, G.W., Fulton, R.C., Cooper, A.S.: Phys. Rev. B **11**, 440 (1975)
26. McElfresh, M.W., Hall, J.H., Ryan, R.R., Smith, J.L., Fisk, Z.: Acta. Cryst. **C46**, 1579 (1990)
27. Hidaka, H., Nagata, R., Tabata, C., Shimizu, Y., Miura, N., Yanagisawa, T., Amitsuka, H.: Phys. Rev. Materials **2**, 053603 (2018)
28. Niemann, S., Jeitschko, W.: J. Solid State Chem. **114**, 337 (1995)
29. Hacher Jr, H., Lin, M.S.: Solid State Commun. **6**, 37 (1968)
30. Mizumaki, M., Tsutsui, S., Iga, F.: J. Phys. Conf. Ser. **176**, 012034 (2009)

31. Trounov, V.A., Malyshev, A.L., Chernyshov, D.Yu., Korsukova, M.M., Gurin, V.N., Aslanov, L.A., Chernyshev, V.V.: J. Phys. Condens. Matter **5**, 2479 (1993)
32. Mandrus, D., Sarrao, J.L., Lacerda, A., Migliori, A., Thompson, J.D., Fisk, Z.: Phys. Rev. B **49**, 16809 (1994)
33. Tsutsui, S. et al. unpublished
34. Alekseev, P.A., Ivanov, A.S., Dorner, B., Schober, H., Kikoin, K.A., Mischenko, A.S., Lazukov, V.N., Konovalova, E.S., Paerno, Y.B., Runyantsev, A.Y., Sadikov, I.P.: Europhys. Lett. **10**, 457 (1989)
35. Tsutsui, S., Hasegawa, T., Takasu, Y., Ogita, N., Udagawa, M., Yoda, Y., Iga, F.: J. Phys. Conf. Ser. **176**, 012033 (2009)